Oxygen Reduction on Silver Low-Index Single-Crystal Surfaces in Alkaline Solution: Rotating Ring Disk$_{Ag(hkl)}$ Studies

B. B. Blizanac,* P. N. Ross, and N. M. Marković

Materials Sciences Division, Lawrence Berkeley National Laboratory, University of California, Berkeley, California 94720

Received: October 21, 2005; In Final Form: December 21, 2005

The rotating ring disk method is applied to investigate the oxygen reduction reaction on Ag single-crystal surfaces in alkaline solution over the temperature range 293−333 K. At all temperatures, the oxygen reduction reaction proceeds through the $4e^-$ reaction pathway with a very small (≈0.5−2%) peroxide formation. At the same temperature and overpotentials, the kinetics of the ORR always increases in the order (100) ≤ (111) < (110), indicating that the reaction is structure-sensitive. We present an interpretation of the structure sensitivity based on the supposition that it arises from (i) a potential-dependent adsorption of spectator hydroxyl ions and (ii) variations in activation energies, which are determined by the O_2 adsorption on Ag single-crystal surfaces covered by adsorbed oxygenated species.

1. Introduction

The oxygen reduction reaction (ORR) is regarded as one of the most important electrocatalytic reactions because of its role in electrochemical energy conversion systems, several industrial processes, and corrosion. At the metal-solution interface the ORR takes place as a multielectron reaction that is controlled by the delicate balance between the heat of adsorption of O_2 and reaction intermediates and the availability of active metal sites. While the energetic term is uniquely related to the electronic properties of electrode material,[1−3] the number of active metal sites is predominantly determined by a potential-dependent surface coverage of the so-called spectator species such as H_{upd},[4,5] OH_{ad},[6] HSO_4,[5] Cl_{ad},[7] and Br_{ad}.[8] Studies of the ORR on Pt, Au, and Cu single-crystal surfaces showed unambiguously that the reaction is structure-sensitive and that variations in the kinetics with the crystal face are controlled by the structure-sensitive adsorption of spectator species.[3,9] In contrast to Pt(*hkl*), Au(*hkl*),[10−12] and Cu(*hkl*),[13] very little is known about the structure sensitivity of the ORR on Ag single-crystal surfaces. In the very first report, by utilizing the rotating disk electrode (RDE) method Zwetanova and Juttner[14] found that in both acid and alkaline solution the ORR on Ag single crystals is not a structure-sensitive reaction. In contrast, under very similar experimental conditions McIntyre and Peck[15] reported a small difference in activity between low-index single-crystal surfaces of Ag. In agreement with McIntyre and Peck, Isakovic and Adzic[16] found at least a 50 mV difference in the half-wave potential for the ORR on Ag(*hkl*) in acid solutions. While the activity in acid solutions decreased in the sequence Ag(111) > Ag(100) = Ag(110), in alkaline solutions the Ag-(100) plane exhibited the highest catalytic activity.[15] Although it was found that the ORR is dependent on the geometry of Ag surface atoms, none of the previous reports discussed the origin of the observed structure sensitivity.

In this paper, to get further insight into the structure sensitivity of the ORR on Ag(*hkl*), we will use the rotating ring disk electrode (RRDE) method. This method would allow us to monitor simultaneously the ORR on the disk electrode and the formation of peroxide on the ring electrode. We will also show how the kinetics of the ORR and the formation of H_2O_2 depend on the temperature of electrolyte. On the basis of experimental findings that the activation energies for the ORR and adsorption of hydroxyl ions on Ag(*hkl*) are both dependent on a surface geometry, we present an interpretation of the structure sensitivity based on the combination of these two factors.

2. Experimental Section

The Ag(*hkl*) single crystals (0.283 cm^2) were chemically polished before each experiment in a mixture of CrO_3 and HCl according to the procedure based on the work of Hamelin et al.,[17] originally developed from a patent quoted in ref 18. Here we will give just a brief overview. Prior to the polishing, the crystals were kept for ca. 15 min in concentrated H_2SO_4. After rinsing with triply pyrolitically distilled water, the crystals were dipped several times into concentrated $HClO_4$ (only the crystal face that was to be polished was exposed to the acid solution). The crystals were then transferred into the CrO_3−HCl mixture. During this procedure, a white-yellow precipitate is formed on the crystal, which makes the solution cloudy (again, only the surface which was to be polished was exposed to the solution). After rinsing the crystals in triply pyrolitically distilled water, the crystals were immersed into a concentrated ammonia solution for several minutes (ca. 5−10 min). After the rinsing with water, before mounting in the RRDE configuration, the crystals were kept once more for 10−20 min in concentrated H_2SO_4 and rinsed with water. After mounting in the RRDE setup, the electrodes were transferred into a thermostated standard three-compartment electrochemical cell and immersed into the Ar-purged electrolyte at ≈293 K (Ar, Bay Gas research purity; 0.1 M KOH, Aldrich semiconductor grade prepared with triply pyrodistilled water) under potentiostatic control at ≈−0.2 V. The reference electrode was a saturated calomel electrode (SCE) separated by a closed electrolyte bridge from the working electrode compartment in order to avoid contamination. All potentials, however, refer to that of the reversible hydrogen

* Corresponding author. E-mail: bblizanac@lbl.gov.

10.1021/jp056050d CCC: $33.50
Published on Web 02/22/2006

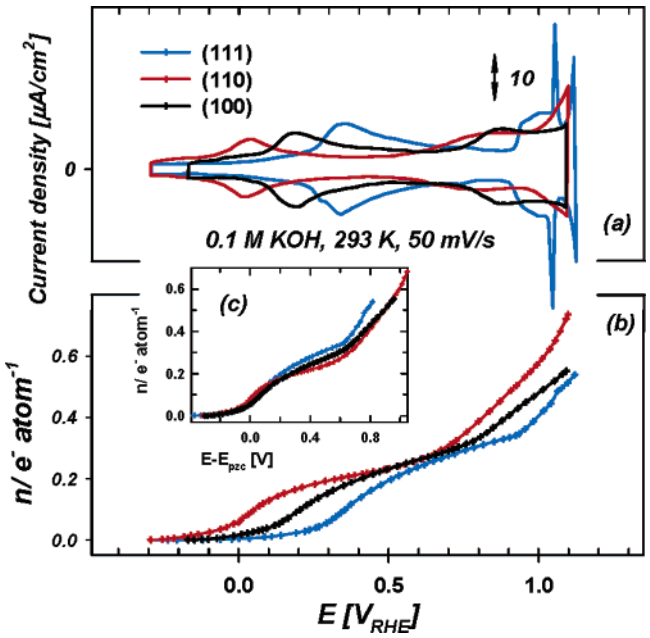

Figure 1. (a) Cyclic voltammetry curves in argon-purged 0.1 M KOH electrolyte on Ag(hkl) surfaces. All cyclic voltammograms were obtained at room temperature with a sweep rate of 50 mV/s. (b) Fractional charge per atom, obtained by integrating the anodic sweep direction of cyclic voltammetry (from a) after accounting for the different surface atom density of different Ag(*hkl*) orientations. (c) Fractional charge per atom expressed on the rational potential scale (RPS).

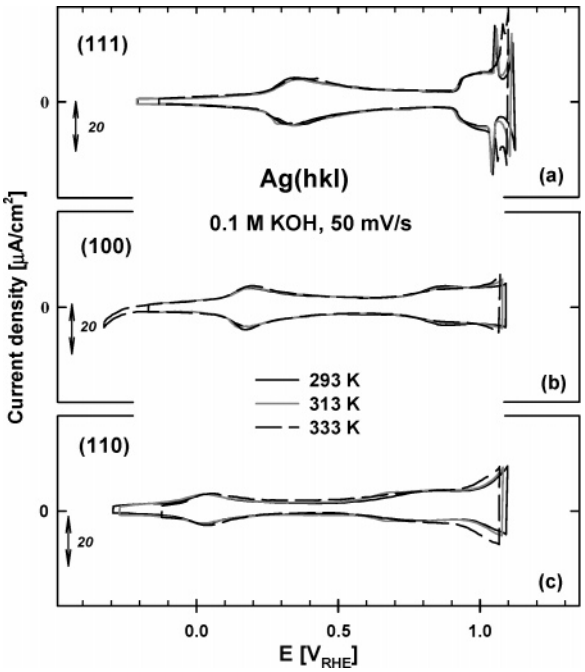

Figure 2. Cyclic voltammetry curves in argon-purged 0.1 M KOH electrolyte on Ag(*hkl*) surfaces at three different temperatures employed in this study (293, 313 and 333 K). All cyclic voltammograms were obtained at a sweep rate of 50 mV/s.

electrode (RHE) in the same electrolyte. The collection efficiency of the RRDE setup was $N = 0.22 \pm 5\%$.

3. Results and Discussion

(3.1) Cyclic Voltammetry. *(3.1.1) Cyclic Voltammetry at Room Temperature.* Cyclic voltammetry (CV) for each crystal face of Ag was recorded in 0.1 M KOH with a sweep rate of 50 mV/s (Figure 1a). All three $i-E$ curves are very similar with previously published voltammograms for Ag(*hkl*) in alkaline electrolytes,[19−22] proving that single crystals embedded in a ring disk configuration are clean and of good quality.

An important observation inferred from Figure 1a is that all three cyclic voltammograms display a very high degree of reversibility in the potential region below bulk Ag_2O formation (0.342 V_{SHE}; 1.18 V_{RHE} in 0.1 M KOH). After a relatively flat current−potential profile at most negative potentials, corresponding to charging/discharging of a double layer, broad reversible anodic/cathodic peaks related to the initial adsorption of OH are stretching up to the third potential region, where additional OH adsorption serves as a precursor for the bulk oxide formation. For each orientation, the total charge density transferred through the metal/electrolyte interface (Q [μC/cm^2]) was obtained by integrating corresponding CV in an anodic sweep direction, after subtracting the charge density required for the charging of the double layer. From this value, and on the basis of the respective surface atom density of Ag(*hkl*) surfaces, a fractional charge per atom (σ_M) was assessed. Considering that the degree of surface coverage by OH (θ_{OH}) is proportional to the fractional charge transferred through the metal/electrolyte interface, from hereafter the $\sigma_M = (E)$ dependence will be referred to as the "OH adsorption isotherm". In Figure 1b, therefore, the OH adsorption isotherms are expressed as the number of electrons passed through a single surface atom as a function of potential. If OH^- anions are fully discharged upon adsorption, then the numeric scale on the *y*-axis is, in fact, a fractional surface coverage of 1 monolayer of OH, where 1 monolayer corresponds to the one OH_{ad} species adsorbed per one Ag surface atom (for different opinions regarding the degree of OH^- discharge upon adsorption see refs 23-27). As illustrated in Figure 1b, the shape of OH adsorption isotherms is structure-insensitive; i.e., a slow initial rise of θ_{OH} is followed first by a steep increase in OH surface coverage, then with a plateau, and, finally with a new steep increase in θ_{OH}. Assuming the same degree of OH^- discharge upon adsorption on all three Ag(*hkl*) surfaces, Figure 1b suggests almost the same OH_{ad} saturated surface coverage on all three surfaces (ca. 0.35 monolayer for fully discharged OH). An important difference between "adsorption isotherms" on Ag (*hkl*) is in the potential shift in the onset of OH adsorption. As was recently shown by Horswell et al.,[22] adsorption isotherms on these three single-crystal surfaces coincide when compared on a rational potential scale (RPS), which accounts for the difference in the potential of zero charge (pzc) for these surfaces. Adsorption isotherms based on rational potential scale are shown in Figure 1c. On the basis of the above analysis, it is reasonable to conclude that the onset of OH adsorption is strongly dependent on the potential of zero charge of Ag single-crystal surfaces, and thus on the work function.

(3.1.2) Cyclic Voltammetry at Elevated Temperatures. Surprisingly, temperature elevation does not have any (or at least any significant) influence on adsorption/desorption processes in the potential range of −0.3 to ca. 1 V, as can be seen from the Figure 2. At $E > 1.0$ V, by increasing the temperature a negative potential shift of the (still reversible) oxide formation is observed.

The fact that cyclic voltammetry of silver single-crystal electrodes does not depend on the temperature (at least within the temperature range used in this work) has one very important implication—oxygen reduction reaction at all temperatures proceeds at (almost) the *same* surface coverage by OH_{ad}.

(3.2) Oxygen Reduction Measurements. *(3.2.1) Oxygen Reduction Reaction at Room Temperature.* An indispensable

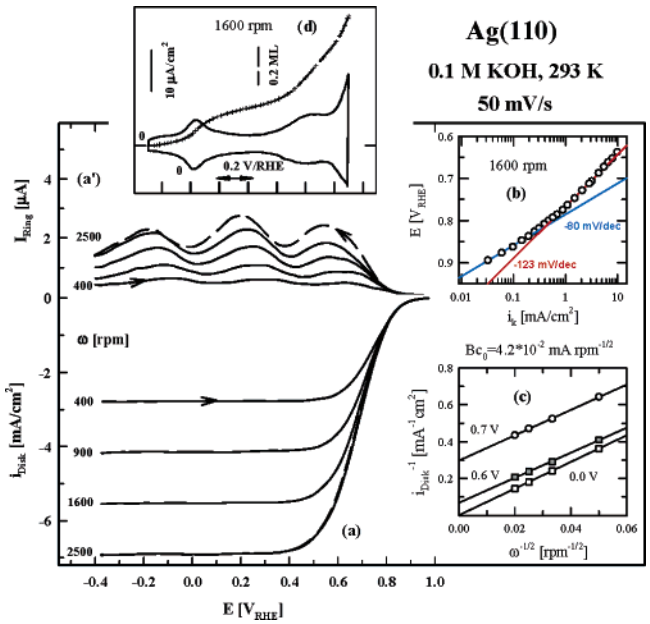

Figure 3. Current−potential cuves at 293 K for ORR in oxygen-saturated 0.1 M KOH solution for the ring electrode (a′) and for the disk electrode (a) of Ag(110) at various rotation rates; (b) mass-transport-corrected currents with extrapolated Tafel slopes for lcd and hcd regions; (c) Levich plot, inferred from a, at different potentials; (d) cyclic voltammetry on Ag(110) at 50 mV/s under 1600 rpm along with the "OH adsorption isotherm".

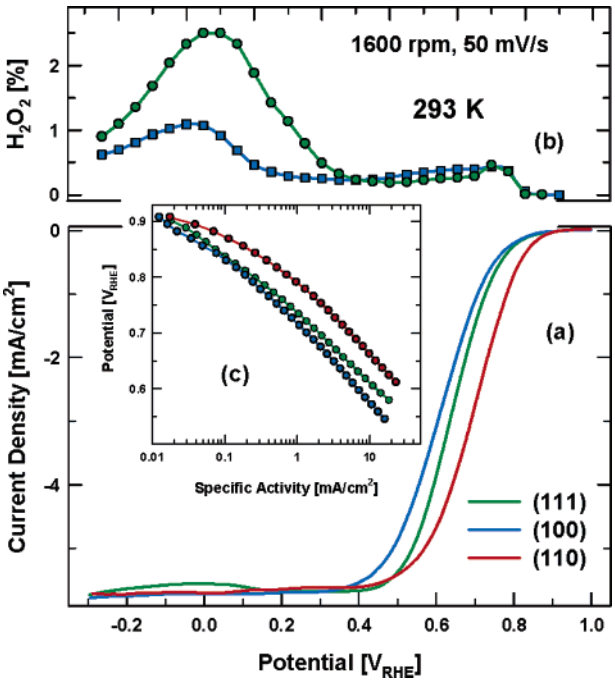

Figure 4. (a) Current−potential curves for ORR in 0.1 M KOH at 293 K on different Ag(*hkl*) single-crystal orientations; (b) peroxide production for two extreme cases; (c) mass-transport-corrected currents for ORR at all three orientations.

method in any kinetics study that involves gas reactants with a very low solubility is the rotating ring disk electrode (RRDE) method. This method provides conditions where forced convection allows continuous supply of O_2 to the electrode surface, thereby enabling the determination of catalytic activity that is free of diffusion limitations. Although the current−potential curves for the O_2 reduction were obtained in the same manner for all three single-crystal surfaces, for our purposes here a complete set of results and analysis will be shown only for the ORR on the Ag(110) surface. Kinetic parameters for the two other surfaces were assessed from a similar analysis.

Figure 3a shows that the potential region of a kinetic control ($0.65 < E < 0.95$ V) and a combined kinetic−diffusion control ($0.5 < E < 0.65$ V) is followed by a pure diffusion limiting current for the ORR. The production of H_2O_2 on the disk electrode is monitored on the ring electrode at $E_{ring} = 1.2$ V, i.e., at the potential where H_2O_2 oxidation is diffusion-limited. As shown in Figure 3a′, throughout the potential region between 0.8 and −0.4 V, the corresponding ring currents were a very small fraction of the disk current, indicating that the ORR proceeds almost entirely through the $4e^-$ pathway. The $4e^-$ reduction is confirmed from the analysis of Levich plots, i.e., from a slope of the i^{-1} vs $\omega^{-0.5}$ curve in Figure 3c. Given that the experimental value of the so-called B factor (slope of the Levich plot, $B = 4.2 \times 10^{-2}$ mA rpm$^{-0.5}$) agrees very well with the theoretical value of $B = 4.27 \times 10^{-2}$ mA rpm$^{-0.5}$ for the four-electron reduction {the later calculated by using literature data for O_2 solubility (1.26×10^{-3} mol/dm^3),[6] viscosity (1.09×10^{-2} cm^2/s),[6] and oxygen diffusivity (1.93×10^{-5} cm/s) [6]}, we concluded that indeed $4e^-$ are exchanged in the ORR on Ag(110) in alkaline solution. Note that the Levich plot at 0.0 V intercepts the i^{-1} axis at the origin, proving that the current at this potential is indeed entirely diffusion-limited, as stated previously. Interestingly, Figure 3a shows that there is almost no hysteresis between polarization curves recorded in positive- and negative-going sweep directions. The same behavior was observed also on the other two Ag(*hkl*) orientations. This is significantly different from the ORR current on Pt low-index single-crystal surfaces,[5,6] where significant current hysteresis between the anodic and cathodic sweeps is observed. It has been proposed that this current hysteresis is controlled by the formation of an irreversible platinum oxide at $E > 0.6$ V.[6] The fact that O_2 reduction currents on Ag(*hkl*) are insensitive to the sweep direction is a further conformation that the OH adsorption on these surfaces is a reversible process; see Figure 1 and Figure 2.

Figure 3b shows that the Tafel plot of mass transport corrected currents for the ORR on the Ag(110) surface increases monotonically with the overpotential. Depending on the method of drawing the tangent through the points of what appears to be a continuous curve, one might extrapolate any Tafel slope between ca. 80 and 120 mV/decade. In our case, we somewhat arbitrarily fitted the curve with two slopes: a low Tafel slope (80 mV/decade) obtained by fitting a tangent to the polarization curve at low overpotentials, i.e., $0.8 < E < 0.9$ V where $I/I_d \sim 0.05$, and a high Tafel slope (123 mV/decade) from the tangent fitted through points on the polarization curve at high overpotentials, $0.65 < E < 0.85$ V. Tafel slopes, extrapolated from the analysis of polarization curves for the other two Ag(*hkl*) electrodes, using the same procedure have a similar range of values.

Polarization curves for the ORR on all three single-crystal planes at 298 K are compared in Figure 4 (positive sweep direction at 1600 rpm and with 50 mV/s). A close inspection of Figure 4 reveals that the structure sensitivity for O_2 reduction is rather small (at least much smaller than on Pt(*hkl*)), yet clearly discernible, with the (110) surface being the most active and the (100) surface the least active for the ORR. This result is in agreement with previous findings that the difference in catalytic activity between different single-crystal surfaces of Ag in alkaline solution is small, ca. 50 mV. In addition to the previous RDE data, however, our results, depicted in the upper panel of Figure 4, show that a production of peroxide on all three single

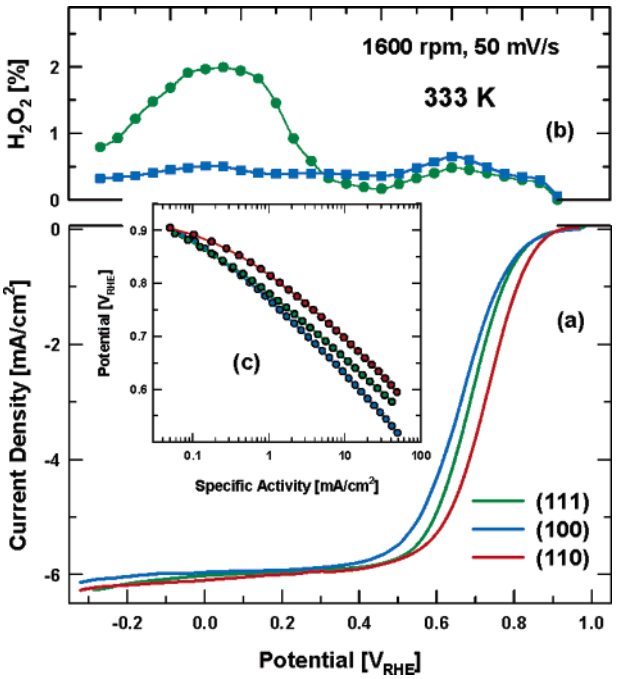

Figure 5. (a) Current−potential curves for ORR in 0.1 M KOH at 333 K on different Ag(*hkl*) single-crystal orientations; (b) peroxide production for two extreme cases; (c) mass-transport-corrected currents for ORR at all three orientations.

crystals is small, ranging from 0.5% at low overpotentials to 1−2.5% at high overpotentials.

Further analysis of Figure 4 indicates that the main difference in peroxide production on Ag(*hkl*) occurs in the potential region where the ORR is under a pure diffusion control, whereas in the region of mixed kinetic−diffusion control peroxide formation is practically structure-insensitive. The structure sensitivity of the ORR on Ag(*hkl*) can also be observed from the Tafel slopes, which are summarized in the insert of Figure 3. Similarly to that for the Ag(110) surface, for the other two single-crystal orientations the Tafel slope is continuously changing from 70−80 to 120−130 mV/decade. From the insert of Figure 4, for the kinetic current density of 0.3 mA/cm^2 activity increases in the order (110) > (111) ≥ (100), in contrast to previos reports,[15] the (100) surface being ≈80 mV less active from the most active (110) plane.

(3.2.2) Oxygen Reduction Reaction at Elevated Temperatures. The shape of the polarization curves for the oxygen reduction reaction at 333 K is almost identical with one obtained at 293 K; i.e., the region of mixed kinetic−diffusion control is followed by a well-defined plateau for a diffusion-limited oxygen reduction process. Analysis of the Levich plots (not shown) revealed that the ORR proceeds through the 4e$^-$ reaction pathway ($B = 4.0 \times 10^{-2}$ mA rpm$^{-0.5}$) with a very small (≈0.5−2%) peroxide formation.

Polarization curves for all three single-crystal surfaces at 333 K, along with peroxide production, are summarized in Figure 5. As at 293 K, the rate of the ORR at 333 K increases in the order Ag(110) > Ag(111) ≥ Ag(100). In agreement with results at low temperature, at 333 K peroxide production at low overpotentials ($0.6 < E < 0.8$ V) is low (≈0.5%) and structure-insensitive. At higher overvoltages ($E > 0.6$ V), however, the peroxide yield is the highest (≈2%) on the (111) surface, whereas on the other two crystal faces is ≈1%. Comparison between Figures 4 and 5 indicates that by increasing the temperature from 293 to 333 K, the rate of the ORR increases by a factor of ca. 2, as well as that the amount of H_2O_2 is

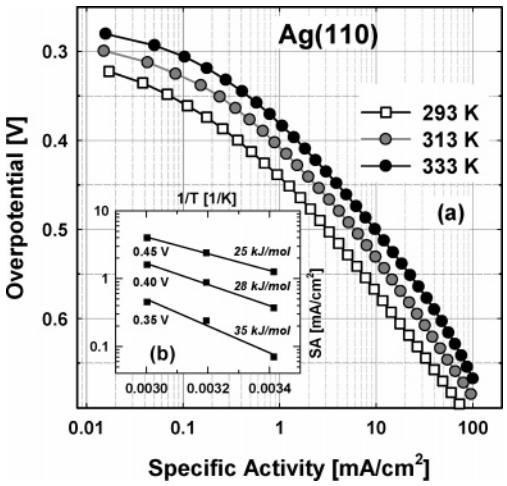

Figure 6. (a) Mass-transport-corrected current−potential curves for oxygen reduction reaction on Ag(110) at different temperatures; (b) Arrhenius plots at different fixed overpotentials calculated by using eq 2.

reduced at elevated temperature. The insert of Figure 5 shows the Tafel plots for the ORR on Ag(*hkl*) in alkaline solution at 333 K. Again, as at 293 K, values for the Tafel slopes on all three surfaces are almost the same: i.e., a low Tafel slope of ≈70 mV/decade and a high Tafel slope of ≈130 mV/decade.

(3.2.3) Apparent Activation Energies. An important part of kinetic analysis is determination of the apparent activation energies (ΔE^*), which in the case of the ORR can be determined from Arrhenius equation at constant overpotentials:[28−30]

$$\left.\frac{\partial(\log i_k)}{\partial(1/T)}\right|_{\eta} = \frac{\Delta E^*}{2.3R} \qquad (1)$$

The overpotential with respect to the O_2/H_2O equilibrium potential at each temperature, η_{O_2}, is determined from the potential measured at reversible hydrogen electrode scale at the respective temperature, $E_{RHE}(T)$, and the reversible H_2/O_2 cell potential, $E_{cell}(T)$:

$$\eta_{O_2}(T) = E_{cell}(T) - E_{RHE}(T) = \frac{-\Delta G_{H_2/O_2}(T)}{2F} - E_{RHE}(T) \qquad (2)$$

where the temperature dependence of $\Delta G_{H_2}/O_2(T)$ is given by

$$\Delta G_{H_2/O_2}(T) = -295600 - 33.5T \ln T + 388.4T \lfloor \text{J mol}^{-1} \rfloor \qquad (3)$$

It has been shown that the deviations of the reversible H_2/O_2 cell potential due to a decrease in oxygen partial pressure with increasing temperature are negligible in the temperature range of 298−333 K.[30]

The apparent activation energies for the ORR on each Ag(*hkl*) face were obtained at three different overpotentials from three different temperatures using the Arrhenius plot. Again, we use a set of mass-transport-corrected current−potential curves for the ORR on Ag(110) at different temperatures to demonstrate the temperature effects on kinetics of the ORR.

As expected, Figure 6 shows that the kinetics of the ORR is enhanced at elevated tempertures. In the insert (b) of Figure 6 is shown the Arrhenius dependence for three different ovepotentials, 0.35, 0.4, and 0.45 V. Not surprisingly, because at higher overpotentials the activation barrier for the reduction process is reduced, the apparent activation energies decrease by increasing the overpotential; from 35 kJ/mol at 0.35 V to

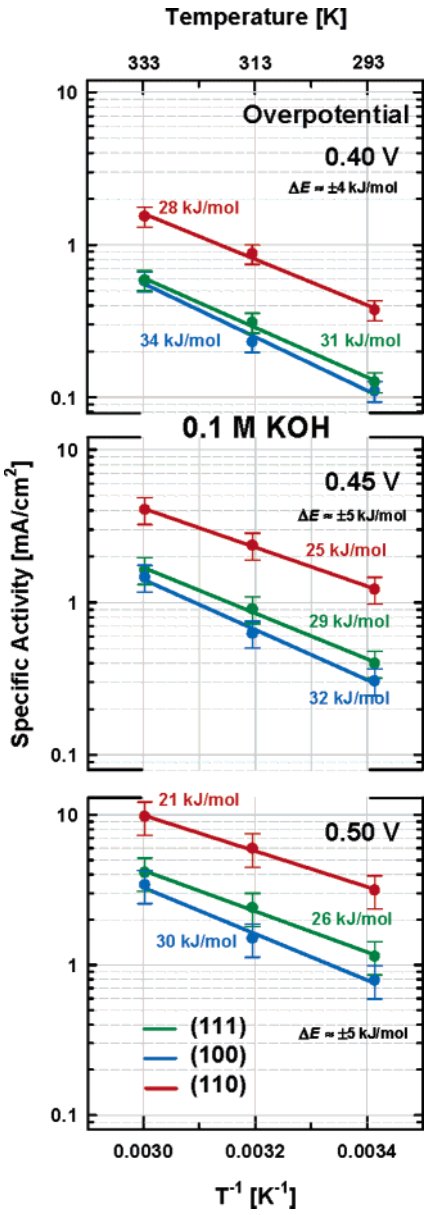

Figure 7. Arrhenius plots of kinetic currents at fixed overpotentials for Ag(*hkl*) over the full range of temperatures employed in this study.

25 kJ/mol at 0.45 V. Values for the apparent activation energies on the other two Ag single-crystal surfaces were extrapolated from similar Arrhenius plots. Apparent activation energies for all three Ag(*hkl*) surfaces at three different overpotentials are summarized in Figure 7. Considering significant error in the determination of apparent activation energy based on measurements on three different temperatures only, the absolute values, at this point, are of no particular interest. However, based on these results, there is small, yet discernible, dependence of the apparent activation energy on crystallographic orientation. Furthermore, regardless of the applied overpotential apparent activation energy is always the lowest for the Ag(110) surface and the highest for the Ag(100) surface orientation, with the apparent activation energy for the ORR on the Ag(111) surface between these two. This is, again, different from the apparent activation energy for oxygen reduction reaction on low index platinum single crystals, where activation energy does not depend on crystallographic orientation.

(3.3) Reaction Pathway and Structure Sensitivity. Although there are numerous reaction pathways and schemes proposed for the ORR,[2,16] it appears that the one presented below is the most appropriate for the ORR on the platinum group and IB group metals:[3,12]

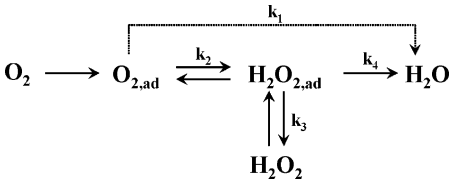

On the basis of this reaction scheme, three reaction pathways are possible. One is direct four-electron O_2 reduction to water (rate constant k_1), where first electron transfer is immediately followed by breaking of the O−O bond (no peroxo intermediates). Second possible pathway is two-electron reduction to H_2O_2 (rate constant k_2), which can be either a final product (rate constant k_3), or further be reduced to water (k_4), i.e., the so-called *serial four-electron pathway*. *Direct* and *serial* four-electron pathways have the same final product, water molecules, and cannot be distinguished by utilizing the rotating ring disk electrode.[16] Nevertheless, the analysis for the ORR on Pt(*hkl*) and Au(*hkl*) single-crystal surfaces supports the serial reaction pathway.[3,12,31] As we demonstrate below, the same pathway is most likely operative on Ag(*hkl*) in KOH.

We will proceed by accepting the hypothesis that the rate-determining step is the first charge-transfer step and the formation of adsorbed superoxide radical anion $^{\bullet}O_{2,ad}^{-}$:

$$O_{2,ad} + e^{-} \rightarrow {}^{\bullet}O_{2,ad}^{-} \qquad (4)$$

Second, if the first electron transfer is the rate-determining step, then, as in the case for the ORR on Pt and Au, the rate of the ORR on Ag can be expressed as

$$i = nFkc_{O_2}(1 - \Theta_{ad})^{x} \exp\left(\frac{-\beta FE}{RT}\right) \exp\left(\frac{-\gamma r\Theta_{ad}}{RT}\right) \qquad (5)$$

where n is the number of electrons, k is the chemical rate constant, c_{O_2} is the concentration of O_2 in the solution, Θ_{ad} is the degree of the total surface coverage by all adsorbed species, x is either 1 or 2 depending on the site requirements of the adsorbates, β and γ are the symmetry factors, r (the so-called Frumkin or Temkin parameter) is a parameter characterizing the rate of change of the free energy of adsorption of reacting intermediates with the surface coverage by (all) adsorbed species, and E is applied potential. On the basis of eq 6, two main factors determine the kinetics of the oxygen reduction reaction: (i) the preexponential, $(1 - \Theta_{ad})$, term determines the active site occupancy by *all* adsorbed species, i.e., it determines the availability of the OH_{ad}^{-}-free Ag sites for adsorption of O_2 and reaction intermediates, and, (ii) the exponential term defines the apparent activation energy for the rate-determining step. In the following sections we will use this reaction pathway and rate expression to analyze the effects of various factors on the kinetics of the ORR on Ag(*hkl*) surfaces in alkaline solution.

Assuming that the coverage of ORR intermediates is low under reaction conditions,[32] in 0.1 M KOH only the OH_{ad} species has to be considered. Then, from eq 5, the corresponding Tafel relationship could be found from the following expression:

$$-\frac{\partial \log i}{\partial E} = \frac{\beta F}{2.3RT} + \left[\frac{x}{(1 - \theta_{OH_{ad}})} + \frac{\gamma r}{RT}\right]\frac{\partial \theta_{OH_{ad}}}{\partial E} \qquad (6)$$

If we, further, assume that the transfer coefficient (β) is

TABLE 1: Tafel Slopes at $\eta = 0.4$ as a Function of Temperature

	Tafel slope at $\eta = 0.4$ V (mV/dec)		
temp (K)	Ag(111)	Ag(100)	Ag(110)
293	93	98	91
313	101	112	106
333	106	123	114

temperature-independent,[31,33−35] then at 293 K the first term should correspond to a Tafel slope of 116 mV/decade. At the constant temperature, the second term may cause the Tafel slope to vary with potential, either through the potential-dependent surface coverage by OH_{ad} or through the change in a value of the Frumkin parameter. Generally, for $r = 0$ (Langmuir behavior) higher θ_{OH} should result in the lower Tafel slope. On the other hand, if $r \neq 0$ (Frumkin behavior), then the energetic term may also contribute to the Tafel slope. For example, from the $\theta_{OH} - E$ dependence the Tafel slope in the lcd region (≈80 mV/decade) can be quantitatively explained by using the following fit parameters: $x = 2$ (two sites required for O_2^- adsorption) and $f = r/RT = 1$, 2, and 4 for the (110), (111), and (100) surfaces, respectively, the latter suggesting relatively strong lateral repulsion between adsorbed OH_{ad} and the reaction intermediates.

As we discussed above, by increasing temperature the Tafel slope should increase from 116 mV/decade at 293 K to 132 mV/decade at 333 K.[31] Since the d(log *i*)/d*E* is continuously changing in the same range (ca. 80−130 mV/decade), it is very difficult to extrapolate the correct values for the Tafel slope. An improved estimate is obtained by drawing a tangent through one point of the d(log *i*)/d*E* curve at the same overpotential. The corresponding results are summarized in Table 1 for all three Ag(*hkl*) surfaces at the overpotential of 0.4 V.

From Table 1, although values of the Tafel slopes differ from the theoretically expected one, the fact that slopes increase by increasing the temperature may indicate that the Tafel slope is proportional to the temperature, with the symmetry factor (β) being independent of temperature.

To explain the structure sensitivity for oxygen reduction reaction as well as the temperature dependence, we will summarize now the two most important findings from previous analysis. First of all, from Figure 1 we learn that in the potential region were O_2 reduction is under mixed kinetic−diffusion conditions, a fractional surface coverage by OH_{ad} is structure-sensitive, being the highest on Ag(110) and the lowest on Ag(111). Second, from Figure 7 we found that activation energies for oxygen reduction reaction are also structure-sensitive and increase in the order Ag(110) < Ag(111) < Ag(100). On the basis of these observations, it is reasonable to suggest that at $T =$ constant the structure sensitivity is determined by the relative contribution of both: preexponential $(1 - \Theta)$ and exponential energetic terms in eq 5. At given potential, surface coverage by OH_{ad} is the highest on the Ag(110) surface, which leads to the lowest number of available Ag sites on which O_2 and reaction intermediates can be adsorbed. On the other hand apparent activation energy is the lowest on this surface, indicating the strongest interaction of O_2 with the (110) symmetry. These two opposing effects are obviously optimized on the (110) surface, and thus Ag(110) is the most active surface for the ORR. On the other hand, a relatively high surface coverage by OH_{ad} species and moderate O_2 chemisorption energy on Ag(100) are determining the lowest activity of the surface atoms with the (100) symmetry. Obviously, the balance between the availability of free Ag sites, the $(1 - \theta)$ term, and energy of adsorption of O_2 (the "ΔG" term) is such that the (111) surface is less active than (110) but more active than (100).

Therefore, we propose the importance of OH_{ad} on the kinetics of the ORR on Ag(*hkl*) similar to the one proposed for the ORR on Pt(*hkl*). The major difference in OH adsorption on Ag(*hkl*) and Pt(*hkl*) surfaces is that whereas the OH_{ad} layer on Ag(*hkl*) is almost ideally reversible, on Pt(*hkl*) the reversible adsorption is followed by an irreversible adsorption of OH_{ad}, which we usually termed an "oxide". The consequence of the reversible/irreversible transition is the appearance of the hysteresis in the current between the anodic and cathodic sweeps, which is not observed on Ag(*hkl*). It appears that the magnitude of hysteresis in polarization curves is in direct correlation with the nature of the $M-OH_{ad}$ interaction. The reversible voltammetric features as well as the lack of hysteresis in the ORR currents on Ag(*hkl*) suggests the $Ag-OH_{ad}$ interaction is much weaker than the $Pt-OH_{ad}$ interaction. This puts Ag in the category of metals with a rather weak $M-OH_{ad}$ bond. The affinity of Ag toward oxygen is, however, strong enough to break the O−O bond and to yield four-electron reduction. This is not surprising, considering that in the gas-phase dissociative adsorption of O_2 is observed on silver surfaces even at room temperature.[36]

Conclusions

Results for the ORR on low-index single-crystal Ag(*hkl*) surfaces in alkaline solution over the temperature range of 293−333 K have been presented. At all temperatures, oxygen reduction reaction proceeds as the serial $4e^-$ reaction pathway with a very small peroxide formation. The order of activity of Ag(*hkl*) in 0.1 M KOH has increased in the sequence (110) > (111) ≥ (100). The structure sensitivity remains the same at all temperatures employed in this study.

Acknowledgment. This work was supported by the Director, Office of Science, Office of Basic Energy Sciences, Division of Materials Sciences, U.S. Department of Energy, under Contract No. DE-AC03-76SF00098.

References and Notes

(1) Appleby, A. J. *Catal. Rev.* **1970**, *4*, 221−244.
(2) Kinoshita, K. *Electrochemical Oxygen Technology*; John Wiley & Sons: New York, 1992.
(3) Markovic, N. M.; Ross, P. N. *Surf. Sci. Rep.* **2002**, *45*, 117−230.
(4) Markovic, N. M.; Adzic, R. R.; Cahan, B. D.; Yeager, E. *J. Electroanal. Chem.* **1994**, *377*, 249−259.
(5) Markovic, N. M.; Gasteiger, H. A.; Ross, P. N. *J. Phys. Chem.* **1995**, *99*, 3411−3415.
(6) Markovic, N. M.; Gasteiger, H. A.; Ross, P. N. *J. Phys. Chem.* **1996**, *100*, 6715−6721.
(7) Stamenkovic, V.; Markovic, N. M.; Ross, P. N., Jr. *J. Electroanal. Chem.* **2000**, *500*, 44−51.
(8) Markovic, N. M.; Gasteiger, H. A.; Grgur, B. N.; Ross, P. N. *J. Electroanal. Chem.* **1999**, *467*, 157−163.
(9) Lucas, C. A.; Markovic, N. M. *Encyclopedia of Electrochemistry*, Vol. 2, Section 4.1.2.1.2; Wiley-VCH: New York, 2004.
(10) Adzic, R. R.; Markovic, N. M.; Vesovic, V. B. *J. Electroanal. Chem.* **1984**, *165*, 105−120.
(11) Markovic, N. M.; Adzic, R. R.; Vesovic, V. B. *J. Electroanal. Chem.* **1984**, *165*, 121−133.
(12) Blizanac, B. B.; Lucas, C.; Gallagher, M.; Arenz, M.; Ross, P. N.; Markovic, N. M. *J. Phys. Chem.* **2003**, *108*, 625−634.
(13) Brisard, G. M.; Bertrand, N.; Ross, P. N.; Markovic, N. M. *J. Electroanal. Chem.* **2000**, *480*, 219−224.
(14) Zwetanova, A.; Juttner, K. *J. Electroanal. Chem.* **1981**, *119*, 149−164.
(15) McIntyre, J. D. E.; Peck, W. F. *Electrochemistry at Single-Crystal Metal Electrodes. Electrocatalytic Effects on Surface Atomic Structure, Defects and Adatoms on Oxygen Reduction*; The Electrochemical Society: Pennington, NJ, 1984; pp 102−130.
(16) Adzic R. R. *Electrocatalysis*; Wiley-VCH: New York, 1998; pp 197−242.

(17) Hamelin, A.; Doubova, L.; Stoicoviciu, L. *J. Electroanal. Chem.* **1988**, *244*, 133−145.
(18) Kurasawa, T. Jpn. Pat. May 23, 1960.
(19) Savinova, E. R.; Scheybal, A.; Danckwerts, M.; Wild, U.; Pettinger, B.; Doblhofer, K.; Schlogl, R.; Ertl, G. *Faraday Discuss.* **2002**, *121*, 181−198.
(20) Jovic, B. M.; Jovic, V. D.; Stafford, G. R. *Electrochem. Commun.* **1999**, *1*, 247−251.
(21) Stevenson, K. J.; Gao, X.; Hatchett, D. W.; White, H. S. *J. Electroanal. Chem.* **1998**, *447*, 43−51.
(22) Horswell, S. L.; Pinheiro, A. N. L.; Savinova, E. R.; Danckwerts, M.; Pettinger, B.; Zei, M. S.; Ertl, G. *Langmuir* **2004**, *20*, 10970−10981.
(23) Horswell, S. L.; Pinheiro, A. L.; Savinova, E. R.; Pettinger, B.; Zei, M. S.; Ertl, G. *J. Phys. Chem. B* **2004**, *108*, 18640−18649.
(24) Savinova, E. R.; Zemlyanov, D.; Scheybal, A.; Scheidel-Niedrig, Th.; Doblhofer, K.; Schlogl, R. *Langmuir* **1999**, *15*, 6546−6551.
(25) Savinova, E. R.; Zemlyanov, D. Y.; Scheybal, A.; Schlogl, R.; Doblhofer, K. *Langmuir* **1999**, *15*, 6552−6556.
(26) Lutzenkirchen-Hecht, D.; Strehblow, H. H. *Electrochim. Acta* **1998**, *43*, 2957−2968.
(27) Hecht, D.; Strehblow, H. H. *J. Electroanal. Chem.* **1997**, *440*, 211−217.
(28) Sepa, D. B.; Vojnovic, M. V.; Vracar, L.; Damjanovic, A. *Electrochim. Acta* **1986**, *31*, 91−96.
(29) Sepa, D. B.; Vojnovic, M. V.; Vracar, L. *Electrochim. Acta* **1986**, *31*, 1105−1111.
(30) Paulus, U. A.; Schmidt, T. J.; Gasteiger, H. A.; Behm, R. J. *J. Electrochem. Soc.* **1999**.
(31) Schmidt, T. J.; Stamenkovic, V.; Ross, P. N.; Markovic, N. M. *Phys. Chem. Chem. Phys.* **2003**, *5*, 400−406.
(32) Tarasevich, M. R. *Electrochimiya* **1973**, *9*, 578.
(33) Appleby, A. J. *J. Electrochem. Soc.* **1970**, *117*, 328−335.
(34) Appleby, A. J. *J. Electrochem. Soc.* **1970**, *117*, 641−645.
(35) Grgur, B. N.; Markovic, N. M.; Ross, P. N., Jr. *Can. J. Chem.* **1997**, *75*, 1465−1471.
(36) Gravil, P. A.; White, J. A.; Bird, D. M. *Surf. Sci.* **1996**, *352*−*354*, 248−252.